European Radiology (2021) 31:4804–4812
https://doi.org/10.1007/s00330-020-07495-0

HEPATOBILIARY-PANCREAS

Noninvasive diagnosis of portal hypertension using gadoxetate DCE-MRI of the liver and spleen

Stefanie J. Hectors[1,2,3] · Octavia Bane[1,2] · Paul Kennedy[1,2] · Jordan Cuevas[1,2] · Swan Thung[4] · Aaron Fischman[2] · Scott L. Friedman[5] · Thomas D. Schiano[5] · Bachir Taouli[1,2]

Received: 16 July 2020 / Revised: 25 September 2020 / Accepted: 10 November 2020 / Published online: 7 January 2021
© European Society of Radiology 2021

Abstract

Objectives To assess the performance of gadoxetate dynamic contrast–enhanced (DCE) MRI of the liver and spleen for noninvasive diagnosis of portal hypertension (PH).

Methods Thirty-five patients (M/F 22/13, mean age 55 years) with chronic liver disease who underwent hepatic venous pressure gradient (HVPG) measurements were prospectively enrolled in this IRB-approved study. All patients underwent multiparametric MRI including gadoxetate DCE-MRI acquisition. Model-based and model-free DCE-MRI analyses were performed. The correlation between DCE-MRI parameters and HVPG was assessed. ROC analysis was employed to determine the diagnostic performance of DCE-MRI parameters alone and in combination for prediction of PH and clinically significant (CS)PH (HVPG > 5 and ≥ 10 mmHg, respectively).

Results Mean HVPG was 7.0 ± 5.0 mmHg (range 0–18 mmHg). Twenty-one (60%) patients had PH, of whom 9 had CSPH. Modeled liver uptake fraction f_i and uptake rate k_i and model-free parameters liver upslope and uptake were all significantly negatively correlated with HVPG (r range − 0.490 to − 0.398, p value range 0.003–0.018), while spleen interstitial fraction v_e was significantly positively correlated with HVPG (r = 0.336, p = 0.048). For PH diagnosis, liver k_i showed the best diagnostic performance with an AUC, sensitivity, and specificity of 0.74 (confidence interval (CI) 0.57–0.91), 71.4%, and 78.6%. The combination of liver k_i and spleen v_e was selected as the best classifier for diagnosis of CSPH with an AUC, sensitivity, and specificity of 0.87 (CI 0.75–0.99), 100%, and 73.1%.

Conclusions Our results demonstrate the potential utility of hepatocyte uptake parameters and spleen interstitial fraction obtained with gadoxetate DCE-MRI for the diagnosis of PH and CSPH.

Key Points

- *Liver uptake and spleen interstitial fraction estimates from gadoxetate DCE-MRI are significantly correlated with portal pressure measurements.*
- *Liver uptake rate shows good diagnostic performance for the diagnosis of portal hypertension.*
- *The combination of liver uptake rate with spleen interstitial fraction exhibits excellent diagnostic performance for the diagnosis of clinically significant portal hypertension.*

Keywords Perfusion imaging · Portal hypertension · Portal pressure · Liver diseases · Liver cirrhosis

✉ Bachir Taouli
bachir.taouli@mountsinai.org

[1] Biomedical Engineering and Imaging Institute, Icahn School of Medicine at Mount Sinai, New York, NY, USA

[2] Department of Diagnostic, Molecular and Interventional Radiology, Icahn School of Medicine at Mount Sinai, 1470 Madison Ave, New York, NY 10029, USA

[3] Department of Radiology, Weill Cornell Medicine, New York, NY, USA

[4] Department of Pathology, Icahn School of Medicine at Mount Sinai, New York, NY, USA

[5] Division of Liver Diseases, Department of Medicine, Icahn School of Medicine at Mount Sinai, New York, NY, USA

Abbreviations

ART	Arterial fraction
CPA	Collagen proportionate area
CSPH	Clinically significant portal hypertension
DCE-MRI	Dynamic contrast–enhanced MRI
F_a	Arterial flow
f_i	Uptake fraction
F_p	Portal flow
F_t	Total flow
HVPG	Hepatic venous pressure gradient
k_i	Intracellular uptake rate
MTT	Mean transit time
PH	Portal hypertension
ROI	Region of interest
SI	Signal intensity
TTP	Time to peak
v_e	Interstitial volume fraction

Introduction

Portal hypertension (PH) is one of the major complications of liver cirrhosis [1], and develops due to intrahepatic resistance to blood flow [2]. PH is associated with severe complications, including ascites, encephalopathy, and bleeding from gastroesophageal varices [3]. It is thus of critical importance that PH is diagnosed in a timely manner in order to avoid these potentially deadly complications.

The definitive diagnosis of PH relies on invasive hepatic venous pressure gradient (HVPG) measurements. While HVPG measurement is highly accurate for the diagnosis of PH (HVPG > 5 mmHg) and clinically significant (CS)PH (HVPG ≥ 10 mmHg), the procedure is invasive, costly, and only available in specialized centers [4]. Therefore, there is an urgent need for noninvasive surrogate measurements for the diagnosis of PH and CSPH.

Several imaging methods for the assessment of PH have been evaluated [5], most notably elastography methods, either ultrasound- [6–8] or MRI-based [9, 10], with promising results. However, limitations of ultrasound elastography include limited signal penetration in patients with obesity or ascites [5]. MR elastography is a relatively costly procedure, which requires additional equipment. In addition, MR elastography is prone to failure in patients with obesity, massive ascites, or iron deposition [11, 12], although failure rates are lower than with ultrasound elastography. Therefore, there remains a need for the development of an accurate, cost-effective method for the diagnosis of PH.

Dynamic contrast–enhanced MRI (DCE-MRI) offers unique capabilities to capture fibrosis-induced changes in the liver [10, 13, 14]. In addition to liver DCE-MRI parameters, spleen DCE-MRI may also be of interest for assessment of PH. Due to increased resistance to outflow of blood from the splenic vein, PH also induces pathological changes in the spleen, including congestion, angiogenesis, and fibrogenesis [15, 16]. DCE-MRI could potentially be sensitive to PH-induced splenic angiogenesis [10].

Several previous studies have evaluated the utility of DCE-MRI parameters for evaluation of PH [10, 13]. These studies quantified perfusion by analysis of contrast dynamics in the first few minutes after contrast injection. DCE-MRI using a liver-specific agent such as gadoxetate provides the unique opportunity to measure both liver perfusion and function within a single DCE-MRI acquisition that includes the delayed phase after contrast [17]. The additional functional parameters derived from gadoxetate DCE-MRI measurements may potentially be more strongly associated with PH compared to conventional DCE-MRI perfusion parameters.

The objective of our study was to assess the performance of liver and spleen quantitative DCE-MRI using gadoxetate for the diagnosis of PH and CSPH.

Materials and methods

Study design

This prospective single-center study was approved by our Institutional Review Board. Signed informed consent was obtained from all patients. Inclusion criteria for our study were as follows: adult patients with liver disease and suspected PH, scheduled for a clinically indicated HVPG measurement within 3 months of MRI (either in combination with a transjugular biopsy or as part of a transjugular intrahepatic portosystemic shunt (TIPS) placement). Exclusion criteria were as follows: history of liver transplant, ongoing beta-blocker treatment, or portal vein occlusion. A total of 36 patients who matched the eligibility criteria were enrolled in our study between March 2018 and January 2020. One patient was excluded because the time between MRI and HVPG measurement exceeded 3 months. Of the final 35 included patients, 22 were male and average age was 55 years (range 22–79 years). Thirty-three patients underwent HVPG measurements, which were indicated due to suspicion of PH. The remaining 2 patients underwent TIPS placement due to refractory ascites. The etiologies of liver disease were as follows: non-alcoholic fatty liver disease/steatohepatitis (NAFLD/NASH), $n = 11$; autoimmune hepatitis, $n = 5$; chronic hepatitis infection C, $n = 4$; primary sclerosing cholangitis, $n = 4$; cryptogenic cirrhosis, $n = 3$; non-cirrhotic portal hypertension, $n = 3$; alcohol- or drug-induced liver disease, $n = 2$; non-specific reactive hepatitis, $n = 2$; hemochromatosis, $n = 1$. The MRI was performed either before or after HVPG measurement. In patients scheduled for TIPS placement, MRI was always performed before the procedure. The average absolute delay between HVPG measurement and MRI was 22 ± 19 days (range 0–78 days).

MRI acquisition

The MRI acquisition was performed at 1.5 T (Aera, Siemens Healthineers) using an 18-channel flexible body coil and a 32-channel integrated spine coil. Patients were instructed to fast for at least 6 h prior to the MRI examination to eliminate postprandial effects on the MRI quantification [18]. Standard abdominal MRI acquisitions included axial and coronal T_2-weighted HASTE acquisitions; multi-echo Dixon for liver fat and iron quantification; T_1-weighted VIBE before and at 1, 3, 10, and 20 min after contrast injection; and diffusion-weighted imaging.

The DCE-MRI data were acquired using a fat-suppressed 3D VIBE acquisition with the following parameters: echo time 1.2 ms, repetition time 2.91 ms, flip angle 11.5°, matrix 256 × 208, field-of-view 380 × 310 mm^2, 44 slices, slice thickness 4 mm, and temporal resolution 4.7 s. DCE-MRI data were acquired for 10 min with brief (10 s) interruptions for clinical T_1-weighted VIBE acquisitions at 1 and 3 min after injection. The contrast agent (gadoxetate disodium, Eovist/Primovist, Bayer Corporation; 10 ml dose; average dose of 0.035 ± 0.008 mmol/kg; range 0.023–0.055 mmol/kg) was injected intravenously at 2 ml/s at 15 s after start of the acquisition, followed by a 30 ml saline flush at the same injection rate.

DCE-MRI analysis

The DCE-MRI analysis was performed by an MRI physicist with 5 years of experience in abdominal MRI analysis. DCE-MRI pre-processing including motion correction and region of interest (ROI) analysis in the liver, spleen, aorta, and portal vein was performed as described previously [10]. Liver DCE-MRI modeling was performed using a dual-input dual-compartment model, which reflects inflow from both the hepatic artery and the portal vein and accumulation of contrast agent in the extracellular space and intracellularly by hepatocyte uptake [17]. The following modeled DCE-MRI parameters were quantified in the liver: arterial plasma flow F_a, portal venous plasma flow F_p, total plasma flow F_t, arterial fraction ART, mean transit time MTT, interstitial volume fraction v_e, intracellular uptake rate k_i, and uptake fraction f_i. A single-input single-compartment model was used for spleen DCE-MRI analysis to estimate F_t, MTT, and v_e. The fitting was performed with different delays between the vascular input functions and the tissue curves, and the fit with the lowest residual error was selected [19].

Model-free parameters were also estimated. In the liver, these parameters were time to peak (TTP), upslope, and uptake. TTP was measured as the time from initial contrast enhancement to peak enhancement, which was defined as the initial peak in the perfusion part of the dynamic liver (CA) curve. Liver upslope was calculated as the slope of the dynamic (CA) curve during this TTP. Liver uptake was calculated as the slope of the (CA) curve between 5 min after injection and the end of the acquisition. For the spleen, TTP and upslope were also estimated. An example of the estimation of model-free parameters is shown in Fig. 1.

HVPG measurement

HVPG measurement was performed as described in a previous report [20]. HVPG was measured by subtracting the free mean pressure from the wedge pressure. Following the HVPG measurement, a transjugular liver biopsy was taken. In two of the patients, a TIPS was placed after the HVPG measurement.

Histopathological analysis

Fibrosis stage and inflammation grade were evaluated from the biopsy specimens by a liver pathologist with more than 20 years of experience. The METAVIR and Brunt (for NASH) scoring systems were used for fibrosis staging and inflammation grading [21, 22]. Fibrosis quantification was also performed by measuring collagen proportionate areas (CPA) based on picrosirius red stains. CPA is defined as the collagen area divided by the total tissue area [23].

Statistical analysis

Statistical analysis was performed in MATLAB (version R2019b, MathWorks) and SPSS (version 20, IBM). Given the small sample size, non-parametric tests were used. The correlation of each of the DCE-MRI parameters with HVPG was assessed using Spearman correlation analysis. The Spearman correlation of DCE-MRI parameters and HVPG with liver pathological fibrosis stage, CPA, and inflammation grade was also evaluated. Differences in DCE-MRI parameters between patients with and without PH (HVPG > 5 mmHg vs. HVPG ≤ 5 mmHg) and with and without CSPH (HVPG ≥ 10 mmHg vs. HVPG < 10 mmHg) [4] were tested with the Mann-Whitney U test. ROC analysis was performed to evaluate the diagnostic performance of the DCE-MRI parameters for assessment of PH, CSPH, and cirrhosis (fibrosis stage F4). Logistic regression with stepwise feature selection was employed to evaluate the potential value of combined DCE-MRI parameters for improved diagnosis of PH, CSPH, and cirrhosis. Only features that showed significance in univariate analysis were included in the logistic regression analysis. For all tests, a significance level of 0.05 was used.

Results

Patients

The mean HVPG was 7.0 ± 5.0 mmHg (range 0–18 mmHg). Twenty-one (60%) patients had PH, of whom 9 (26% of entire

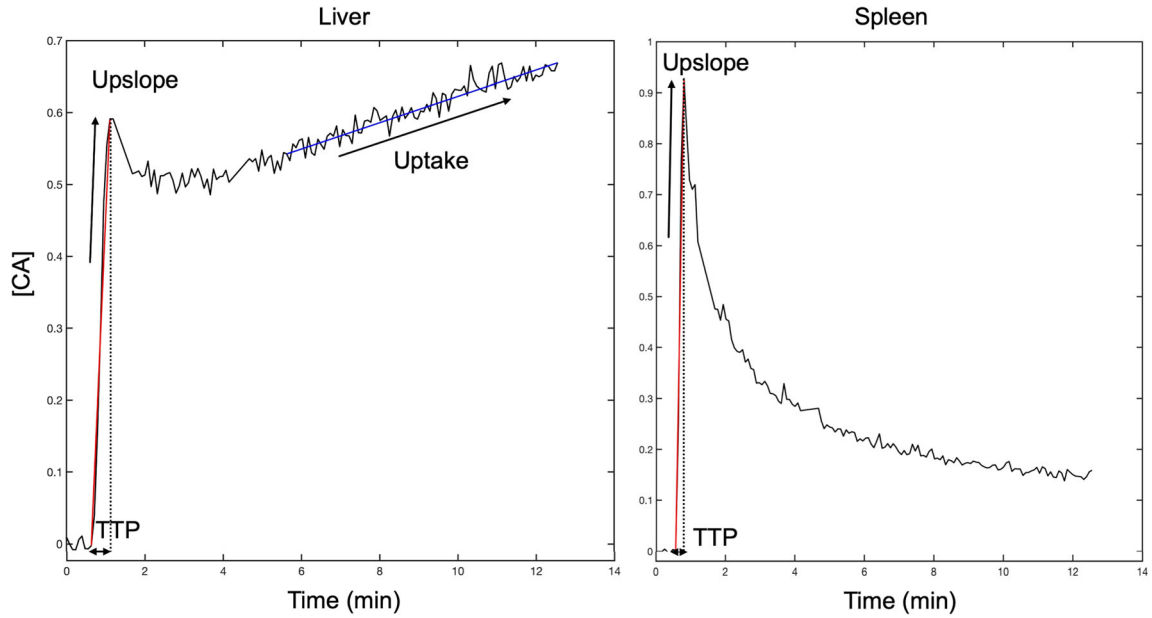

Fig. 1 Estimation of model-free DCE-MRI parameters in the liver and spleen of a 30-year-old female patient with autoimmune hepatitis and no PH (HVPG = 2 mmHg). Time to peak (TTP) was defined as the time to the initial peak in the perfusion part of the curve. The upslope was calculated as the slope of the curve during TTP (red lines). In the liver, uptake was measured as the slope of the curve between 5 min after injection and the end of the acquisition (blue line). For this case, liver upslope, TTP, and uptake were 0.021 mM/s, 28.8 s, and 0.300 * 10^{-3} mM/s, respectively. Spleen upslope and TTP were 0.065 mM/s and 14.4 s, respectively

cohort) had CSPH. The distribution of fibrosis stage was as follows: F0, n = 5 (14%); F1, n = 5 (14%); F2, n = 5 (14%); F3, n = 7 (20%); F4, n = 13 (37%). Inflammation grades were as follows: A0, n = 14 (40%); A1, n = 7 (20%); A2, n = 12 (34%); A3, n = 2 (6%). Among the patients with PH, fibrosis stage was distributed as follows: F0, n = 3 (14%); F1, n = 3 (14%); F2, n = 2 (10%); F3, n = 5 (24%); F4, n = 8 (38%). Of the patients with CSPH, the majority (n = 5, 56%) had liver cirrhosis (stage F4). CPA was successfully quantified in 33 patients, with an average CPA of 0.16 ± 0.13 (range 0.02–0.65). For the remaining 2 patients, there was not sufficient tissue available for the additional collagen staining.

Correlation of DCE-MRI parameters with HVPG and pathology

DCE-MRI acquisition and analysis were successfully performed in all patients. Figure 2 shows contrast-enhanced images and DCE-MRI curves in the liver and spleen for representative patients without PH and with PH and CSPH. With respect to modeled liver DCE-MRI parameters, liver uptake fraction f_i and uptake rate k_i both showed a significant negative correlation with HVPG (r = − 0.482, p = 0.003 and r = − 0.490, p = 0.003, respectively; Fig. 3). Model-free liver parameters upslope and uptake also were significantly negatively correlated with HVPG, but these correlations were slightly weaker than for the modeled parameters (r = − 0.398, p = 0.018 and r = − 0.418, p = 0.012, respectively; Fig. 3). None of the other evaluated liver DCE-MRI parameters correlated with HVPG (p value range 0.113–0.377). In terms of spleen parameters, v_e showed a significant positive correlation with HVPG (r = 0.336, p = 0.048; Fig. 3), while other spleen DCE-MRI parameters showed non-significant correlations (p value range 0.149–0.579).

Liver f_i, k_i, upslope, and uptake were also significantly negatively correlated with liver fibrosis stage (r = − 0.411, p = 0.014; r = − 0.430, p = 0.010; r = − 0.439, p = 0.009; and r = − 0.439, p = 0.008, respectively). In the spleen, F_t and upslope were both significantly negatively correlated with liver fibrosis stage (r = − 0.399, p = 0.018 and r = − 0.504, p = 0.002, respectively), while MTT and TTP were significantly positively correlated with fibrosis stage (r = 0.407, p = 0.015 and r = 0.402, p = 0.017, respectively). The other assessed DCE-MRI parameters did not correlate with fibrosis stage (p value range 0.112–0.549). None of the evaluated liver and spleen DCE-MRI parameters were significantly correlated with inflammation grade (p value range 0.060–0.855). HVPG also did not correlate with fibrosis stage (p = 0.134) nor with inflammation grade (p = 0.792).

Liver ART, f_i, k_i, and uptake were all significantly negatively correlated with CPA (r = − 0.397, p = 0.023; r = − 0.420, p = 0.016; r = − 0.467, p = 0.007 (Fig. 3), and r = − 0.411, p = 0.018, respectively). Spleen DCE-MRI

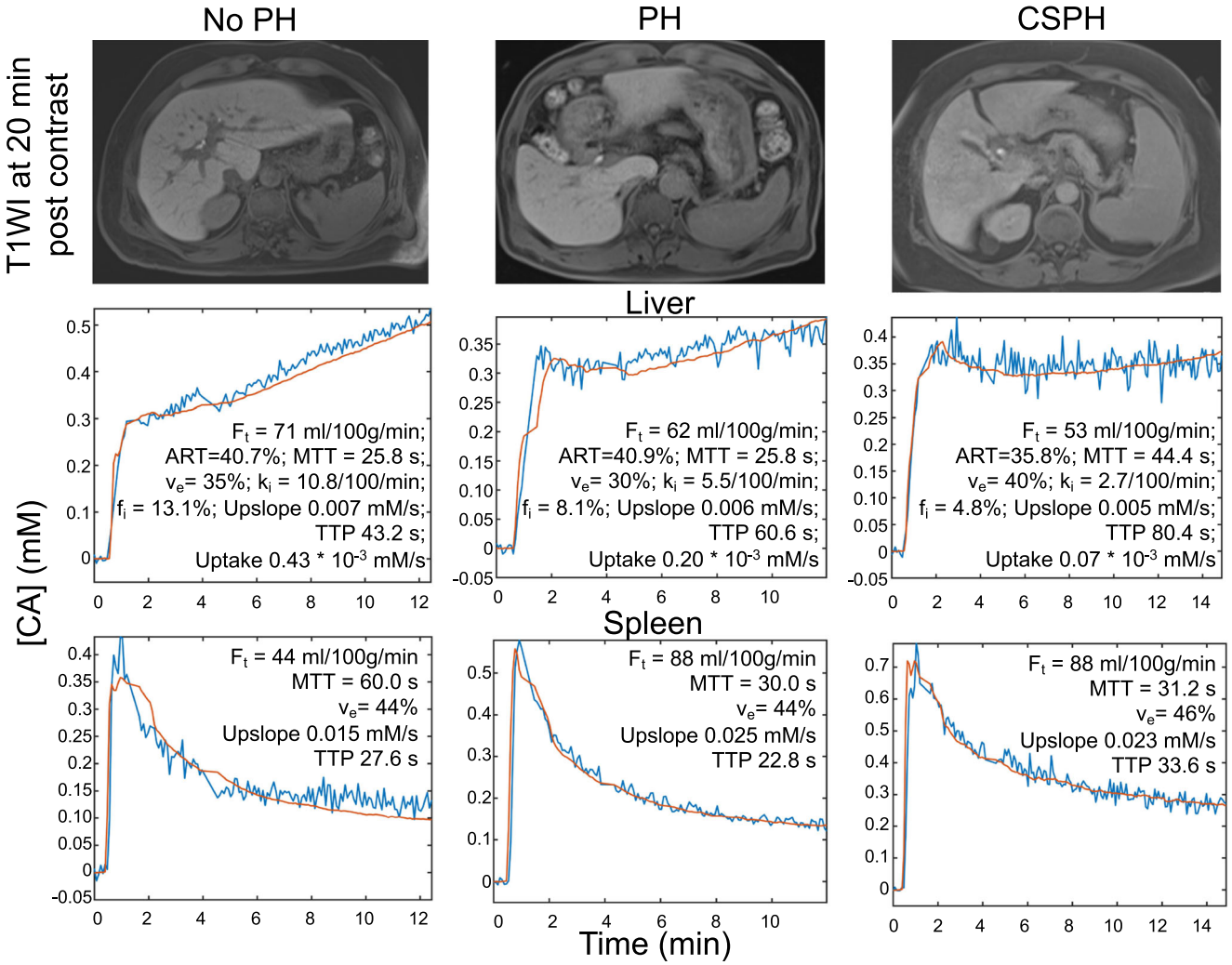

Fig. 2 Liver uptake decreases with portal pressure. Representative post-contrast T_1-weighted images, liver and spleen DCE-MRI data (blue), and fits (red) in (left) a 60-year-old male patient without PH (HVPG = 1 mmHg), (middle) a 72-year-old male patient with PH (HVPG = 9 mmHg), and (right) a 57-year-old male patient with CSPH (HVPG = 17 mmHg). The DCE-MRI parameters are shown in each plot. CSPH, clinically significant portal hypertension; HVPG, hepatic venous pressure gradient; PH, portal hypertension

parameters F_t and MTT were also significantly correlated with CPA ($r = -0.434$, $p = 0.012$ and $r = 0.397$, $p = 0.023$, respectively).

Diagnostic performance for the diagnosis of (CS)PH and cirrhosis

Liver k_i, f_i, and uptake were significantly lower in patients with PH (p value range 0.018–0.038; Table 1). Liver k_i, f_i, uptake, and upslope were all significantly lower in CSPH patients vs. patients with no CSPH (p value range 0.004–0.030; Table 1). In terms of spleen DCE-MRI parameters, v_e and TTP were significantly higher in patients with CSPH vs. no CSPH ($p = 0.009$ and $p = 0.023$, respectively), while upslope was significantly lower in CSPH patients ($p = 0.048$; Table 1). None of the assessed spleen DCE-MRI parameters provided significant differentiation between PH vs. no PH (p value range 0.152–1).

Table 2 shows results of the ROC analysis for diagnosis of PH and CSPH. Liver k_i showed the best diagnostic performance for diagnosis of PH, with an AUC of 0.74 and sensitivity and specificity values of 71.4% and 78.6%, respectively. For the diagnosis of CSPH, liver f_i provided the highest accuracy, with an AUC of 0.83, sensitivity of 77.8%, and specificity of 84.6%.

Liver f_i and uptake were the only parameters that showed significant diagnostic performance for diagnosis of cirrhosis. AUC, sensitivity, and specificity for cirrhosis diagnosis were 0.717 (CI 0.54–0.89, $p = 0.034$), 53.8%, and 86.4% for liver f_i and 0.710 (0.524–0.896; $p = 0.041$), 61.5%, and 81.8% for liver uptake, respectively.

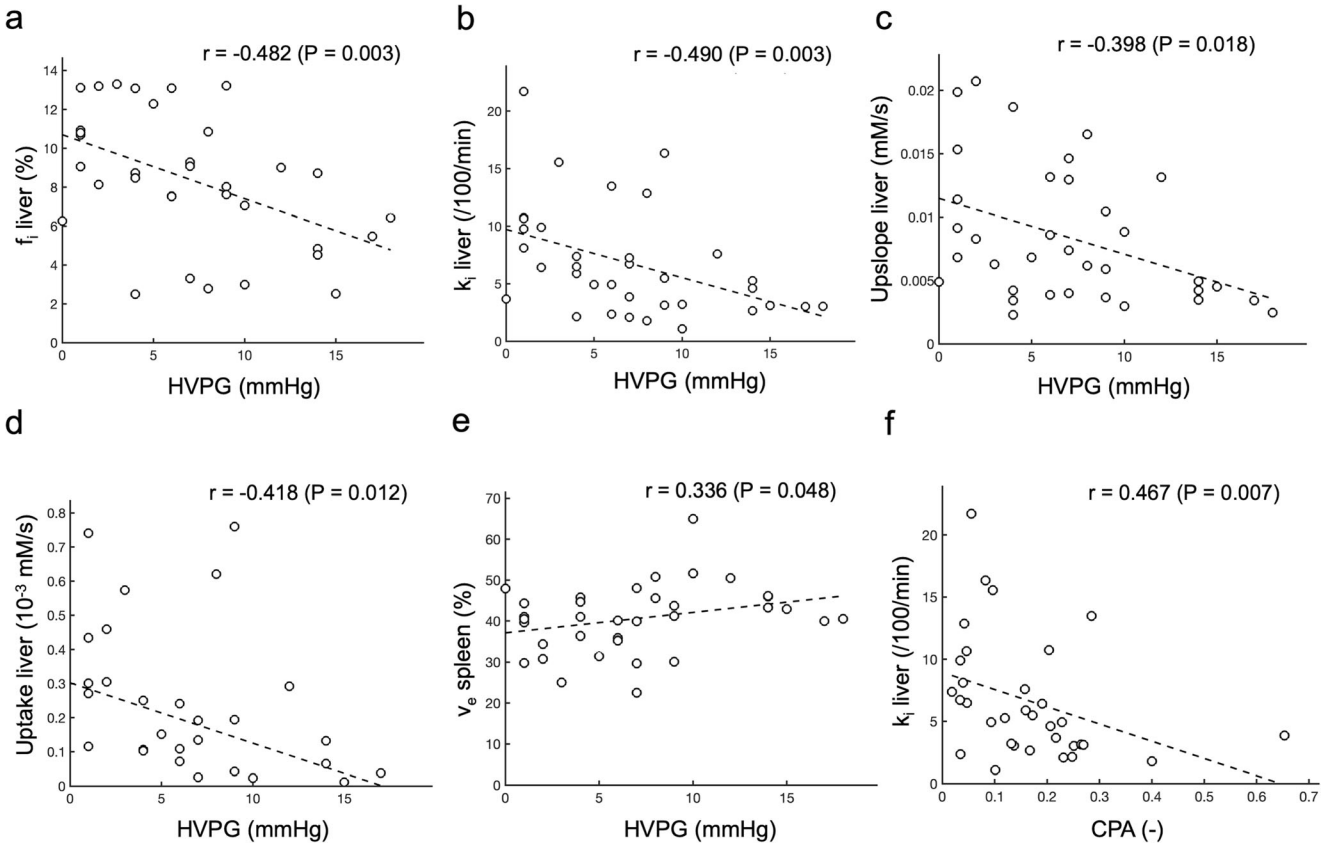

Fig. 3 Correlations plots of (**a**) liver uptake fraction f_i, (**b**) liver uptake rate k_i, (**c**) liver upslope, (**d**) liver uptake, and (**e**) splenic interstitial volume fraction v_e with HVPG, and of (*f*) liver k_i with CPA

Combination of DCE-MRI parameters

Logistic regression with stepwise feature selection did not identify a significant combination of DCE-MRI parameters for the prediction of PH or cirrhosis. However, for the prediction of CSPH, a significant classifier combining liver k_i and spleen v_e was identified ($p < 0.001$), with the following model:

$$\text{logit}(\text{prediction}) = -7.55 - 0.32\, k_{i,\text{liver}} + 0.19\, v_{e,\text{spleen}}$$

This classifier yielded an AUC of 0.87 (confidence interval 0.75–0.99) with a sensitivity of 100% and specificity of 73.1% for the diagnosis of CSPH.

Discussion

In this study, we evaluated the utility of liver and spleen gadoxetate DCE-MRI for the noninvasive assessment of PH. The incremental value of the use of a liver-specific agent for DCE-MRI for PH evaluation is evident by the fact that the strongest correlations with HVPG were observed for uptake parameters k_i and f_i. Liver k_i provided good diagnostic performance (AUC 0.74) for PH diagnosis, while the combination of liver k_i and spleen v_e yielded an excellent performance with an AUC of 0.87 for the diagnosis of CSPH. Modeled DCE-MRI parameters had also stronger correlations with HVPG compared to model-free parameters.

A negative correlation of relative liver enhancement using a clinical contrast-enhanced sequence at a delayed phase after gadoxetate injection with both fibrosis stage [24–26] and HVPG [27] has been reported. The number of functioning hepatocytes is expected to be reduced in advanced fibrosis or cirrhosis, leading to reduced hepatocytic uptake of gadoxetate and thereby lower liver enhancement [28]. In the current study, we also found negative correlations of both k_i and f_i with liver fibrosis stage as well as with CPA. Similar correlations of these parameters with HVPG found in our study indicate that the measured hepatocyte function with gadoxetate DCE-MRI also may approximate the degree of vascular resistance at the sinusoidal level in the liver that causes increased portal pressure [29].

The lack of correlation of modeled DCE-MRI flow parameters in the liver with HVPG observed in our study corresponds to the findings of a previous study [10]. However, another study reported several correlations of liver DCE-MRI flow parameters with portal pressure [13]. The discrepancy between studies may be explained by the overall poor reproducibility and repeatability of liver DCE-MRI flow parameters [19, 30].

Table 1 Liver and spleen DCE-MRI parameters in patients without PH vs. with PH and in patients without CSPH vs. with CSPH

	Parameter	No PH (n = 14)	PH (n = 21)	p	No CSPH (n = 26)	CSPH (n = 9)	p
Liver	Modeled DCE-MRI parameters						
	F_t	76.2 (21.5)	61.0 (36.2)	0.195	68.4 (22.5)	52.3 (38.3)	0.300
	F_a	30.6 (7.7)	22.3 (12.0)	0.126	27.7 (11.3)	20.8 (12.6)	0.317
	F_p	45.1 (14.9)	37.4 (24.2)	0.274	41.1 (14.9)	33.5 (25.7)	0.317
	ART	40.8 (2.7)	38.5 (3.0)	0.083	39.6 (2.9)	37.9 (3.8)	0.356
	MTT	25.7 (5.1)	26.8 (17.7)	0.143	26.6 (5.1)	34.1 (18.3)	0.168
	v_e	34.2 (19.0)	35.5 (14.2)	0.602	34.2 (17.8)	37.3 (9.5)	0.748
	k_i	7.7 (4.8)	3.9 (3.9)	*0.018*	6.6 (6.8)	3.1 (1.9)	*0.017*
	f_i	10.7 (4.6)	7.5 (4.3)	*0.021*	9.1 (4.7)	5.5 (3.3)	*0.004*
	Model-free DCE-MRI parameters						
	Upslope	0.008 (0.010)	0.006 (0.007)	0.259	0.008 (0.008)	0.004 (0.003)	*0.030*
	TTP	60.4 (40.1)	60.4 (41.5)	0.459	60.0 (40.1)	69.3 (23.6)	0.200
	Uptake	0.26 (0.33)	0.07 (0.19)	*0.038*	0.17 (0.23)	0.03 (0.12)	*0.025*
Spleen	Model DCE-MRI parameters						
	F_t	149.0 (141.9)	110.1 (81.5)	0.579	146.8 (87.8)	110.1 (51.2)	0.281
	v_e	40.0 (12.9)	42.9 (7.7)	0.152	40.0 (12.9)	46.0 (8.5)	*0.009*
	MTT	12.2 (19.0)	19.8 (19.6)	0.162	13.4 (19.1)	27.5 (20.2)	0.057
	Model-free DCE-MRI parameters						
	Upslope	0.04 (0.05)	0.04 (0.03)	0.579	0.05 (0.05)	0.03 (0.02)	*0.048*
	TTP	19.1 (14.3)	14.3 (9.0)	> 0.99	14.3 (4.8)	19.1 (15.5)	*0.023*

Data are presented as median (interquartile range). Significant p values are in italics

ART, arterial fraction (%); *CSPH*, clinically significant portal hypertension; F_a, arterial flow (ml/100 g/min); f_i, uptake fraction (%); F_p, portal flow (ml/100 g/min); F_t, total flow (ml/100 g/min); k_i, uptake rate ($(100/\text{min})^{-1}$); *MTT*, mean transit time (s); *PH*, portal hypertension; *TTP*, time to peak (s); v_e, extravascular extracellular volume fraction (%); Upslope (mM/s); Uptake (10^{-3} mM/s)

Imaging parameters in the spleen may directly reflect PH-induced pathophysiological changes in the spleen, without dependency on the underlying liver disease [31]. While we expected to see increased blood flow in the spleen due to PH-

Table 2 ROC analysis of DCE-MRI parameters for the diagnosis of PH and CSPH

	Diagnosis of PH					Diagnosis of CSPH				
	AUC (95% CI)	p	Threshold	Sens (%)	Spec (%)	AUC (95% CI)	p	Threshold	Sens (%)	Spec (%)
Liver										
Modeled parameters										
F_t	0.633 (0.443–0.822)	0.189	64.0	61.9	71.4	0.620 (0.386–0.853)	0.291	57.8	66.7	76.9
F_a	0.656 (0.465–0.848)	0.121	27.7	71.4	71.4	0.615 (0.389–0.842)	0.308	21.5	66.7	76.9
F_p	0.612 (0.422–0.802)	0.266	41.1	66.7	64.3	0.615 (0.376–0.855)	0.308	35.1	66.7	76.9
ART	0.677 (0.493–0.861)	0.080	38.6	52.4	85.7	0.607 (0.371–0.843)	0.345	37.9	55.6	80.8
MTT	0.650 (0.461–0.839)	0.138	25.9	76.2	57.1	0.658 (0.417–0.899)	0.163	34.2	55.6	84.6
v_e	0.646 (0.463–0.830)	0.148	47.6	90.5	28.6	0.538 (0.344–0.733)	0.734	43.2	100.0	38.5
k_i	0.741 (0.572–0.911)	*0.017*	5.7	71.4	78.6	0.774 (0.612–0.935)	*0.016*	5.4	88.9	65.4
f_i	0.735 (0.557–0.912)	*0.020*	8.1	61.9	85.7	0.825 (0.685–0.965)	*0.004*	7.3	77.8	84.6
Model-free parameters										
Upslope	0.616 (0.418–0.813)	0.252	0.006	57.1	71.4	0.748 (0.563–0.933)	*0.029*	0.005	77.8	73.1
TTP	0.577 (0.382–0.771)	0.449	78.4	28.6	100	0.647 (0.430–0.865)	0.193	61.7	77.8	65.4
Uptake	0.711 (0.529–0.893)	*0.037*	0.246	85.7	57.1	0.756 (0.584–0.929)	*0.024*	0.068	77.8	76.9
Spleen										
Modeled parameters										
F_t	0.558 (0.354–0.761)	0.567	146.8	71.4	57.1	0.624 (0.436–0.812)	0.274	144.2	88.9	53.8
v_e	0.646 (0.463–0.830)	0.148	41.1	57.1	71.4	0.799 (0.645–0.953)	*0.008*	39.9	100	50.0
MTT	0.643 (0.441–0.845)	0.157	13.4	76.2	64.3	0.718 (0.545–0.891)	0.163	18.8	88.9	61.5
Model-free parameters										
Upslope	0.442 (0.237–0.647)	0.567	0.044	61.9	50.0	0.726 (0.556–0.897)	*0.045*	0.037	77.8	69.2
TTP	0.503 (0.296–0.711)	0.973	19.1	42.9	71.4	0.756 (0.597–0.916)	*0.024*	0.234	88.9	57.7

Significant p values are in italics

ART, arterial fraction (%); *AUC*, area under the curve; *CI*, confidence interval; *CSPH*, clinically significant portal hypertension; F_a, arterial flow (ml/100 g/min); f_i, uptake fraction (%); F_p, portal flow (ml/100 g/min); F_t, total flow (ml/100 g/min); k_i, uptake rate (100/min); *MTT*, mean transit time (s); *PH*, portal hypertension; *TTP*, time to peak (s); v_e, extravascular extracellular volume fraction (%); Upslope (mM/s); Uptake (10^{-3} mM/s)

induced angiogenesis [15], this was not found in our study, nor in a previous study [10]. We did however observe increased v_e in the spleen, which was also observed as a trend in the other study [10]. The higher splenic v_e in PH may potentially be due to a larger extracellular compartment in the presence of splenic fibrosis due to the accumulation of extracellular matrix components [15, 32].

While no combination of DCE-MRI parameters was identified for the diagnosis of PH, combined liver k_i and spleen v_e was identified as an optimal classifier for the diagnosis of CSPH. These two parameters provide complementary information regarding liver function and PH-induced splenic pathological changes, which may yield improved diagnostic performance of CSPH that needs to be validated in an independent study. Such study could also incorporate other imaging biomarkers for PH for potentially further improved diagnostic accuracy, such as elastography [9, 10], spleen relaxometry parameters $T_{1\rho}$ [20], and iron-corrected T_1 [33] that have shown promise for noninvasive evaluation of PH.

The modeled liver DCE-MRI parameters using the dual-input dual-compartment model were in the same order of magnitude as reported previously [17]. However, flow parameters in both the liver and spleen were substantially lower than in a previous DCE-MRI study in PH patients that used gadobenate dimeglumine as contrast agent, which has a weak uptake in hepatocytes [10]. A possible explanation for this difference in flow could be that a lower dose of contrast agent was used in our study. A higher dose may lead to erroneous estimation of the arterial input function, due to various factors including T_2* and inflow effects [34]. In addition, the previous study used a single-compartment model instead of the dual-compartment model, which may also explain discrepancies in flow estimation.

For clinical application, a disadvantage of the DCE-MRI method may be the time-consuming analysis, requiring image registration and manual ROI segmentation. Several motion-robust abdominal DCE-MRI sequences have been introduced [35, 36], which may be employed to obviate the requirement of image registration. Ultimately, the DCE-MRI analysis itself may also be automated. Recently, a deep learning algorithm for fully automated brain DCE-MRI analysis has been reported [37], which could possibly be adapted to application in abdominal DCE-MRI.

Our study had several limitations. First, sample size was relatively small in this initial study. Our results need to be confirmed in a validation study. Second, there was a variable time interval between the HVPG measurements and the MRI scan, as it was logistically not feasible to schedule the research MRI exam on the same day as the HVPG procedure. Nevertheless, it would not be expected to change over such a short period of time in clinically stable patients. Third, there was high variability in etiology of liver disease, which reflects clinical practice. The influence of etiology on DCE-MRI parameter quantification needs further evaluation. Fourth, we did not evaluate robustness of the DCE-MRI evaluation in terms of reproducibility and repeatability. Finally, we did not assess the presence of gastroesophageal varices in this study.

In conclusion, our results demonstrate the potential utility of hepatocyte uptake parameters and spleen interstitial fraction obtained with gadoxetate DCE-MRI for the diagnosis of both PH and clinically significant PH. These findings require validation in an independent cohort.

Funding This research was supported by NIDDK grant R01DK113272.

Compliance with ethical standards

Guarantor The scientific guarantor of this publication is Bachir Taouli.

Conflict of interest The authors of this manuscript declare no relationships with any companies whose products or services may be related to the subject matter of the article.

Statistics and biometry No complex statistical methods were necessary for this paper.

Informed consent Written informed consent was obtained from all subjects (patients) in this study.

Ethical approval Institutional Review Board approval was obtained.

Study subjects or cohorts overlap Twenty-five of the included patients have been previously reported in Hectors et al Splenic T1ρ as a noninvasive biomarker for portal hypertension. J Magn Reson Imaging. doi: 10.1002/jmri.27087.

Methodology
- prospective
- observational
- performed at one institution

References

1. Bosch J, Garcia-Pagan JC (2000) Complications of cirrhosis. I. Portal hypertension. J Hepatol 32:141–156
2. Turco L, Garcia-Tsao G (2019) Portal hypertension: pathogenesis and diagnosis. Clin Liver Dis 23:573–587
3. de Franchis R, Baveno VF (2010) Revising consensus in portal hypertension: report of the Baveno V consensus workshop on methodology of diagnosis and therapy in portal hypertension. J Hepatol 53:762–768
4. Garcia-Tsao G, Abraldes JG, Berzigotti A, Bosch J (2017) Portal hypertensive bleeding in cirrhosis: risk stratification, diagnosis, and management: 2016 practice guidance by the American Association for the study of liver diseases. Hepatology 65:310–335
5. Qi X, Berzigotti A, Cardenas A, Sarin SK (2018) Emerging noninvasive approaches for diagnosis and monitoring of portal hypertension. Lancet Gastroenterol Hepatol 3:708–719
6. Elkrief L, Rautou PE, Ronot M et al (2015) Prospective comparison of spleen and liver stiffness by using shear-wave and transient elastography for detection of portal hypertension in cirrhosis. Radiology 275:589–598

7. Kim TY, Jeong WK, Sohn JH, Kim J, Kim MY, Kim Y (2015) Evaluation of portal hypertension by real-time shear wave elastography in cirrhotic patients. Liver Int 35:2416–2424
8. You MW, Kim KW, Pyo J et al (2017) A meta-analysis for the diagnostic performance of transient elastography for clinically significant portal hypertension. Ultrasound Med Biol 43:59–68
9. Ronot M, Lambert S, Elkrief L et al (2014) Assessment of portal hypertension and high-risk oesophageal varices with liver and spleen three-dimensional multifrequency MR elastography in liver cirrhosis. Eur Radiol 24:1394–1402
10. Wagner M, Hectors S, Bane O et al (2018) Noninvasive prediction of portal pressure with MR elastography and DCE-MRI of the liver and spleen: preliminary results. J Magn Reson Imaging 48:1091–1103
11. Choi SL, Lee ES, Ko A et al (2020) Technical success rates and reliability of spin-echo echo-planar imaging (SE-EPI) MR elastography in patients with chronic liver disease or liver cirrhosis. Eur Radiol 30:1730–1737
12. Wagner M, Corcuera-Solano I, Lo G et al (2017) Technical failure of MR elastography examinations of the liver: experience from a large single-center study. Radiology 284:401–412
13. Annet L, Materne R, Danse E, Jamart J, Horsmans Y, Van Beers BE (2003) Hepatic flow parameters measured with MR imaging and Doppler US: correlations with degree of cirrhosis and portal hypertension. Radiology 229:409–414
14. Dyvorne HA, Jajamovich GH, Bane O et al (2016) Prospective comparison of magnetic resonance imaging to transient elastography and serum markers for liver fibrosis detection. Liver Int 36:659–666
15. Bolognesi M, Merkel C, Sacerdoti D, Nava V, Gatta A (2002) Role of spleen enlargement in cirrhosis with portal hypertension. Dig Liver Dis 34:144–150
16. Mejias M, Garcia-Pras E, Gallego J, Mendez R, Bosch J, Fernandez M (2010) Relevance of the mTOR signaling pathway in the pathophysiology of splenomegaly in rats with chronic portal hypertension. J Hepatol 52:529–539
17. Sourbron S, Sommer WH, Reiser MF, Zech CJ (2012) Combined quantification of liver perfusion and function with dynamic gadoxetic acid-enhanced MR imaging. Radiology 263:874–883
18. Jajamovich GH, Dyvorne H, Donnerhack C, Taouli B (2014) Quantitative liver MRI combining phase contrast imaging, elastography, and DWI: assessment of reproducibility and postprandial effect at 3.0 T. PLoS One 9:e97355
19. Hectors SJ, Wagner M, Besa C et al (2016) Intravoxel incoherent motion diffusion-weighted imaging of hepatocellular carcinoma: is there a correlation with flow and perfusion metrics obtained with dynamic contrast-enhanced MRI? J Magn Reson Imaging 44:856–864
20. Hectors SJ, Bane O, Stocker D et al (2020) Splenic T1rho as a noninvasive biomarker for portal hypertension. J Magn Reson Imaging. https://doi.org/10.1002/jmri.27087
21. Brunt EM, Janney CG, Di Bisceglie AM, Neuschwander-Tetri BA, Bacon BR (1999) Nonalcoholic steatohepatitis: a proposal for grading and staging the histological lesions. Am J Gastroenterol 94:2467–2474
22. Bedossa P, Poynard T (1996) An algorithm for the grading of activity in chronic hepatitis C. The METAVIR Cooperative Study Group. Hepatology 24:289–293
23. Calvaruso V, Burroughs AK, Standish R et al (2009) Computer-assisted image analysis of liver collagen: relationship to Ishak scoring and hepatic venous pressure gradient. Hepatology 49:1236–1244
24. Verloh N, Probst U, Utpatel K et al (2019) Influence of hepatic fibrosis and inflammation: correlation between histopathological changes and Gd-EOB-DTPA-enhanced MR imaging. PLoS One 14:e0215752
25. Verloh N, Utpatel K, Haimerl M et al (2015) Liver fibrosis and Gd-EOB-DTPA-enhanced MRI: a histopathologic correlation. Sci Rep 5:15408
26. Georgiou L, Penny J, Nicholls G et al (2017) Quantitative assessment of liver function using gadoxetate-enhanced magnetic resonance imaging: monitoring transporter-mediated processes in healthy volunteers. Invest Radiol 52:111–119
27. Asenbaum U, Ba-Ssalamah A, Mandorfer M et al (2017) Effects of portal hypertension on gadoxetic acid-enhanced liver magnetic resonance: diagnostic and prognostic implications. Invest Radiol 52:462–469
28. Tamada T, Ito K, Higaki A et al (2011) Gd-EOB-DTPA-enhanced MR imaging: evaluation of hepatic enhancement effects in normal and cirrhotic livers. Eur J Radiol 80:e311–e316
29. McConnell M, Iwakiri Y (2018) Biology of portal hypertension. Hepatol Int 12:11–23
30. Aronhime S, Calcagno C, Jajamovich GH et al (2014) DCE-MRI of the liver: effect of linear and nonlinear conversions on hepatic perfusion quantification and reproducibility. J Magn Reson Imaging 40:90–98
31. Berzigotti A, Ashkenazi E, Reverter E, Abraldes JG, Bosch J (2011) Non-invasive diagnostic and prognostic evaluation of liver cirrhosis and portal hypertension. Dis Markers 31:129–138
32. Luetkens JA, Klein S, Traber F et al (2018) Quantification of liver fibrosis at T1 and T2 mapping with extracellular volume fraction MRI: preclinical results. Radiology 288:748–754
33. Levick C, Phillips-Hughes J, Collier J et al (2019) Non-invasive assessment of portal hypertension by multi-parametric magnetic resonance imaging of the spleen: a proof of concept study. PLoS One 14:e0221066
34. Jajamovich GH, Calcagno C, Dyvorne HA, Rusinek H, Taouli B (2014) DCE-MRI of the liver: reconstruction of the arterial input function using a low dose pre-bolus contrast injection. PLoS One 9:e115667
35. Feng L, Axel L, Chandarana H, Block KT, Sodickson DK, Otazo R (2016) XD-GRASP: golden-angle radial MRI with reconstruction of extra motion-state dimensions using compressed sensing. Magn Reson Med 75:775–788
36. Qiu W, Li D, Jin X et al (2019) Sliding motion compensated low-rank plus sparse (SMC-LS) reconstruction for high spatiotemporal free-breathing liver 4D DCE-MRI. Magn Reson Imaging 58:56–66
37. Nalepa J, Ribalta Lorenzo P, Marcinkiewicz M et al (2020) Fully-automated deep learning-powered system for DCE-MRI analysis of brain tumors. Artif Intell Med 102:101769

Publisher's note Springer Nature remains neutral with regard to jurisdictional claims in published maps and institutional affiliations.